CFD Analysis of Drag Coefficient of a Parachute in a Steady and Turbulent Condition in Various Reynolds Numbers

Conference Paper · January 2009

DOI: 10.1115/FEDSM2009-78483

2 authors, including:

Mazyar Dawoodian
Gyeongsang National University
15 PUBLICATIONS **118** CITATIONS

SEE PROFILE

Proceedings of the ASME 2009 Fluids Engineering Division Summer Meeting
FEDSM2009
August 2-6, 2009, Vail, Colorado USA

FEDSM2009-78483

CFD ANALYSIS OF DRAG COEFFICIENT OF A PARACHUTE IN A STEADY AND TURBULENT CONDITION IN VARIOUS REYNOLDS NUMBERS

Muhammad Javad Izadi
Azad Islamic University of Takestan
Takestan, Iran
Mj_izadi@yahoo.com

Mazyar Dawoodian
Azad Islamic University of Takestan
Takestan, Iran
Mazyar_dawoodian@yahoo.com

ABSTRACT

Study of parachutes is very important in aerospace industry. In this research, the effect of various Reynolds numbers on a parachute with a vent and without a vent at the top on drag coefficient in a steady and turbulent condition is studied. After a complete research on an efficient grid study, the drag coefficients are calculated numerically. The Reynolds number is varied from 78000 to 3900000 (1 m/s to 50 m/s). It is found that, for a parachute without a vent at the top, as the Reynolds number is increased from 78000 to 800000, the drag coefficient is decreased from about 2.5 to 1.4, and then as the Reynolds number is increased to 1500000, the drag coefficient increased to about 1.62 and it stayed constant for higher Reynolds number up to 3900000. As the vent ratio of the parachute is increased from zero to 5 percent of the parachute inlet diameter, the drag coefficient increased and for further increase of the vent ratio diameter, the drag coefficient decreased, but the general variation of drag coefficient was the same as of same parachute with no vent.

Keywords: Parachute, Wake, Vent, Drag coefficient, Turbulent and CFD Analysis

INTRODUCTION

The dynamics study of bluff bodies involves the consideration of complex aerodynamics phenomena such as semi wake and vortex shedding. This analysis and modeling of wake is useful, when comparing the numerical and experimental results. In this paper several numerical simulations of a hemispherical shell with a vent diameter at its apex in several Reynolds numbers are studied.

Our purpose is to find the effect of various Reynolds numbers and also the effect of vent diameter on drag coefficient, and also the flow field around the body. This finding may be useful in parachute design and its applications. The numerical technique is based on a numerical solution of the 3D Navier-Stocks equations, using the finite volume techniques. For stability and convergence to a solution, we have used the 1st order implicit formulation.

In order to find a general solution, the cross sectional area of our hemi-spherical cup as a reference area is taken to be unity. The body condition is considered isentropic and the flow surrounding the body is to be air. Body surface is without porosity and therefore is taken as rigid. In all of the solutions, the fluid structure interaction is ignored. The primary purpose is to obtain the drag coefficient as a function of the vent diameter ratio (Ratio of the vent to the hemi-spherical cup diameter) for different Reynolds numbers. The second purpose is the validation of the written code by comparing the numerical results against the results obtained by Strickland.

NOMENCLATURE

A	Area
a	Acceleration
c	Sonic Velocity
d	Canopy Diameter
D	Vent Diameter
f	Force
g	Gravity acceleration
M	Mach number
m	Mass
n	Normal direction to the wall surface
p	Pressure
R	Gas constant
T	Temperature
t	Time
u	Velocity Component in X direction
U_∞	Free stream velocity
v	Velocity Component in Y direction

V	Velocity
V_T	Terminal Velocity
w	Velocity Component in Z direction
Greek Symbols	
ρ	Air density
μ	Viscosity
ϕ	Potential function
γ	Specific heat capacity ratio

GOVERNING EQUATIONS:

Let us consider a specific three dimensional and temporary domain. The spatial and temporary coordinates are denoted by $\vec{z} = (x, y, z)$, and $t \in (0, T)$

The Navier-Stokes equations of 3D flows:

$$\frac{\partial \rho}{\partial t} + \nabla . \left(\rho \vec{V} \right) = 0 \tag{1}$$

$$\frac{\partial (\rho u)}{\partial t} + \nabla . \quad \rho u \vec{V} \quad = \quad \frac{\partial p}{\partial x} + \rho f_x + (\quad _x)_{vis} \tag{2-A}$$

$$\frac{\partial (\rho v)}{\partial t} + \nabla . \left(\rho v \vec{V} \right) = -\frac{\partial p}{\partial y} + \rho f_y + (\Im_y)_{vis} \tag{2-B}$$

$$\frac{\partial (\rho w)}{\partial t} + \nabla . \left(\rho w \vec{V} \right) = -\frac{\partial p}{\partial z} + \rho f_z + (\Im_z)_{vis} \tag{2-C}$$

Here f, and $\Im$ are the external body forces, and the viscous forces respectively. For the problem under consideration, the fluid assumed Newtonian, and the flow is taken at first to be laminar and then turbulent and steady. When taken turbulent, the dynamics viscosity of flow is modified locally using a standard k-epsilon turbulent model. No slip boundary condition is applied to the body of the hemi-spherical cup, and the normal velocity on all surfaces of the body is forced to be zero also.

Therefore on all the body surfaces:

$$\vec{V} . n = 0 \tag{3}$$

$$\frac{\partial (\phi)}{\partial n} = 0 \tag{4}$$

DIFFERENTIAL EQUATIONS:

The differential equation of hemispherical shell or generally the hemi-spherical cup problem is based on Newtonian mechanics:

$$\sum \vec{F} = m \vec{a} \tag{5}$$

$\sum F$ And a are all forces on the body and acceleration respectively. In the natural coordinate system in which y is vertical distance above the earth's surface: $a = \frac{dV}{dt}$, and $V = \frac{dz}{dt}$, and therefore we have:

$$\vec{F} = m \frac{d\vec{V}}{dt} \tag{6}$$

In a practical hemi-spherical cup problem, the force "F" is the sum of the gravitational force and drag force. Gravitational force is $F_g = mg$, and the drag force is dependent on the Reynolds number. When, $\mathrm{Re} < 10^3$ the viscous forces dominate and drag force on a solid sphere or the drag force is approximately linear with velocity, and therefore $F_d = 6\pi\mu r V$. This approximation is also known as the creeping flow approximation. When, $\mathrm{Re} > 10^3$. the inertial forces dominate and the drag force and it is approximately proportional with the quadratic of velocity, and therefore: $F_d = 0.5 \rho C_d A U_\infty^2$

Here C_d is the drag coefficient. However, if the downward direction of hemi-spherical cup is taken to be positive, then:

$$F_g - F_d = ma \tag{7}$$

$$K = 0.5 \rho C_d A \tag{8}$$

Now, we define the terminal velocity as the impact velocity. For $\mathrm{Re} > 10^3$ and with a constant velocity (Terminal velocity), equation (7) is as following:

$$mg - kV^2 = m \frac{dV}{dt} = 0 \tag{9}$$

$$k = \frac{mg}{V_T^2} = \frac{mg}{U_\infty^2} \tag{10}$$

Before looking at a numerical approximation to the solution, the constant k can be determined directly from equation (10) by considering the falling hemi-spherical cup velocity either constant or equal to the terminal velocity. For a fixed terminal velocity and a constant area of hemi-spherical cup, k will be a constant coefficient and in this work for every Reynolds number it is known.

PROBLEM SETUP:

In this section the procedure for solving the problem is described. The Figure (l) shows a hemispherical Shell in the Cartesian coordinate systems. The body that is shown in this figure has a vent of air at its apex. Structure or the hemi-spherical cup is considered solid and moving down or the velocity direction is in the positive z direction. The flow

velocity is equal to the terminal velocity, and taken in the range of $1\frac{m}{s} \le V_T \le 50\frac{m}{s}$.

The flow condition is considered as standard condition. So, the air density is then taken to be, $\rho = 1.25\, kg/m^3$, the flow viscosity to be, $\mu = 1.7894 \times 10^{-5}$, and the free stream temperature to be, $T = 288.16\, ^\circ K$ as the reference values. Projected area on the X-Z plane is considered to be unity or equal to $1m^2$. This value will be the reference value for all of the bodies and does not change as the vent ratio varies. Our primary goal is to show the drag coefficient variation as a function of the Reynolds number.

The drag coefficient is dependent on the hemi-spherical cup projected area (πR_o^2), and the free stream velocity U_∞. Also, in this work, the results for five different vent ratios (R_i / R_o) are obtained. To do this, the vent ratio was varied from zero (No vent) to 0.2 (Vent diameter 20 percent of hemi-spherical cup diameter) in several steps. In this numerical work, the flow is taken to be steady and turbulent.

To start the numerical procedure, we must determine the values of the Reynolds numbers, and the Mach numbers:

$$\mathrm{Re} = \rho U_\infty d / \mu \tag{11}$$

$$M = U_\infty / c \tag{12}$$

$$c = \sqrt{\gamma RT} \tag{13}$$

Here c is the sonic velocity and the property of air as an ideal gas is γ, and is equal to 1.4, and after inserting the known values of the above variables in the above equations, we have:

$$\mathrm{Re}_{\min} = \frac{1.25 \times 1 \times 1.128379167}{1.7894 \times 10^{-5}} = 0.7879 \times 10^5 \tag{14}$$

$$\mathrm{Re}_{\max} = \frac{1.25 \times 50 \times 1.128379167}{1.7894 \times 10^{-5}} = 3.9395 \times 10^6 \tag{15}$$

$$c = \sqrt{1.4 \times 287 \times 288.16} = 340.27 m/s \tag{16}$$

$$M_{\min} = 1/340.27 = 0.0029 \tag{17}$$

$$M_{\max} = 50/340.27 = 0.1469 \tag{18}$$

Equations (17) and (18) show that M<0.3 and therefore, we can consider the flow as incompressible flow. Equation (14) shows that an inertial force is dominant under viscous forces and therefore;

$$F_d = 0.5 \rho C_d A U_\infty^2 \tag{19}$$

But equation 15 shows that the viscous forces dominant the inertial forces.

MESHING AND SOLUTION:

The computational domain, unstructured mesh and boundary conditions used for the simulation are shown in Figure 2A. Boundary conditions on the sides of the domain far enough from the parachute are taken as velocity inlet, because far enough from the parachute, flow velocities must be equal to the free stream velocity. The magnitude and directions of the velocity at these boundaries are equal to the free stream velocity. The computational domain stretched from 20 diameter lengths in front of the parachute (upstream) to 50 diameter lengths behind of the parachute (downstream), and 10 diameter lengths away from the parachute edges. Near the body (parachute) walls the mesh is smaller, and very close to the body, even smaller meshes is used.

The boundary distances discussed above were changed several times until the drag coefficient results were not changed anymore, and from this several fixed values as the boundary distances from the parachute is found. These distances are kept as constant values throughout the computation.

At all of the numerical simulation, unstructured T-grid mesh consists of 1199653 tetrahedral cells, 142172 triangular wall faces, 2317820 mixed interior faces, and 242119 nodes (Figure 2A). The governing equations are solved using the implicit finite volume method and segregated solver.

The lateral and outlet boundary conditions were considered as outflow boundary and the inlet boundary condition is considered as velocity inlet (Figure 2B).

RESULTS:

Figure 3 shows the drag coefficient as a function of the Reynolds number. This figure shows that, by increasing the Reynolds number from 78000 to approximately 900000 ($\mathrm{Re} = 9 \times 10^5$), the drag coefficient decreases, and by increasing the vent ratio, in this range of Reynolds numbers, the drag coefficient decreases more. Increasing the Reynolds number to approximately $\mathrm{Re} = 20 \times 10^5$, the drag coefficient increases, and by increasing the vent ratio, in this range of Reynolds numbers, first, the drag coefficient increases up to a vent ratio of five percent (D=5%d), and then it decreases continuously for further increase of vent ratio up to twenty percent vent ratio (D=20%d). This can be seen well in Figure 4. This figure shows the variation of drag coefficient as a function of the vent ratio.

Figure 5 shows the variation of drag coefficient as the vent ratios changes, both numerically (Steady and Unsteady), and experimentally done by Strickland. These three curves show the validity of the numerical results for both steady and unsteady against the experimental (unsteady) results.

Figure 6 to 9 indicate the pressure contours and the velocity vector distribution in color in (pa) and (m/s) around and inside the hemispherical shell without and with vent obtained by the numerical calculations. These figures show the variation of the drag coefficient as a function of velocity or the Reynolds number, and the vent ratio. For the velocity between 1 m/s to 15 m/s, there is no wake at the top of the parachute, but there are two wakes inside the parachute. For the velocities of 15 m/s up to 50 m/s, two wakes appear at the top of the parachute that results in an increase in drag or an increase in the drag coefficient. Increasing the velocity up to 20 m/s, the size of the wakes over the parachutes increases as well, but for the

velocities up to 50 m/s, these wakes do not change as much, and they stay almost constant. Generally the vent ratio is the main reason for a decrease of pressure difference over the sides of the parachute, and by increasing the diameter of the vent, the out flux increases, and the pressure difference between the top and the bottom of the parachute decreases. By comparing the pressure contours of the Figures 6B, 7B, 8B and 9B, it can be seen that, by increasing the diameter of the vent, the blue area (low pressure) and red area (high pressure) at the top and the bottom of the parachute, decreases. And this causes a decrease of the drag force and also the drag coefficient (In these four figures the velocity is constant).

CONCLUSION:

In this paper it is focused on the change of the Reynolds number and the vent ratio variation on the drag coefficient of a bluff body representing a solid parachute. The dependency of the wake behind the vented hemi-spherical shell for various Reynolds numbers is studied.

It is found that, for a parachute without a vent at its apex, as the Reynolds number is increased from 78000 to 800000, the drag coefficient is decreased from 2.5 to 1.4, and then as the Reynolds number is increased to 1500000, the drag coefficient increased to about 1.62 and then it stayed constant for further increase of the Reynolds number up to 3900000. As the vent ratio of the parachute is increased from zero to 5 percent of the parachute inlet diameter, the drag coefficient increased, and for further increase of the vent diameter up to 20 percent of the parachute inlet diameter, the drag coefficient decreased. The general variation of the drag coefficient for all vent ratios was the same as of the parachute without a vent.

The pressure contours and the velocity vectors in Figures 6 to 9 show that, as the Reynolds number increases, the wake behind the shell starts to grow. This phenomenon, affects the drag coefficient results. In this study, the numerical results obtained here are compared with the results gained by Strickland, and this shows the validity of the numerical results (Figure 5).

REFERENCES

1-M.J. Izadi and M. mohammadizadeh, 2008, Numerical study of a hemi-spherical cup in a steady, unsteady, laminar and turbulent flow conditions with a vent of air at the top, ASME Fluids Engineering Division Summer Conference Jacksonville Florida, USA August 10-14, 2008

2- C. W. Peterson and J. H. Strickland and H. Higuchi, 1996, The fluid dynamics of parachute inflation.

3- Keith R. Stein and Richard J. Benney, 2001, Fluid-Structure Interactions of a Round Parachute: Modeling and Simulation Techniques, Journal of AIRCRAFT, Vol. 38, No. 5.

4- K. Stein,T. Tezduyar, V. Kumer, S. Sathe,R. Benney, E. Thornburg, C. Kyle and T. Nonoshita 2003, Aerodynamic Interactions Between Parachute Canopies, ASME.

5- Douglas B. Meade and Allan A. Struthers, 1999, Differential Equations in the new Millennium: the Parachute Problem.

6- J. Potvin, L. Esteve, G. Peek, R. Alamai, and J. Little, Wind Tunnel Study of Cruciform Parachutes Folded in Various configurations, Proceeding of the CEAS/AIAA 15th Aerodynamic Decelerator System Technology Conference, AIAA-991739, Toulouse France, 1999.

7- Benney, R. J., Stein, K. R., Leonard, J. W., and Accorsi, M. L., "Current 3-D Structural Dynamic Finite Element Modeling Capabilities," Proceedings of the 14th AIAA Aerodynamic Decelerator Systems Technology Conference, AIAA 97-1506, AIAA, Reston, VA, 1997, pp. 285–303.

8- Stein, K., Benney, R., Kalro, V., Tezduyar, T., Bretl, T., and Potvin, J., "Fluid-Structure Interaction Simulations of a Cross Parachute: Comparisons of Numerical Predictions with Wind Tunnel Data," Proceedings of the Confederation of European Aerospace Societies/AIAA 15th Aerodynamic Decelerator Systems Technology Conference, AIAA 99-1725, AIAA, Reston, VA, 1999, pp. 172–181. Brooks, A. N., and Hughes, T. J. R., "Streamline Upwind/Petrov–Galerkin

9- Formulations for Convection Dominated Flows with Particular Emphasis on the Incompressible Navier–Stokes Equations, "Computer Methods in Applied Mechanics and Engineering, Vol. 32, 1982, pp. 199–259.

10- Tezduyar, T. E., Behr, M., Mittal, S., and Johnson, A. A., "Computation of Unsteady Incompressible Flows with the Stabilized Finite Element Methods-Space-Time Formulations, Iterative Strategies and Massively Parallel Implementations," New Methods in Transient Analysis, edited by P. Smolinski, W. K. Liu, G. Hulbert, and K. Tamma, AMD- Vol. 143, American Society of Mechanical Engineers, New York, 1992, pp. 7–24.

11- B. E. Launder and D. B. Spalding, "The numerical computational of turbulent flow's" Computational Methods Appl. Mech. Eng 3,269-289(1974).

12- F.M.WHITE, FLUID MECHANICS, McGraw-Hill Book Company, 1988.

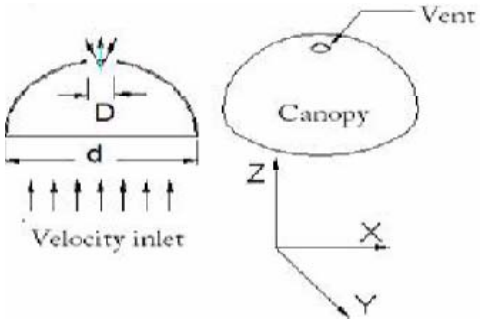

Figure l: Hemispherical shell with a vent in the Cartesian coordinate systems

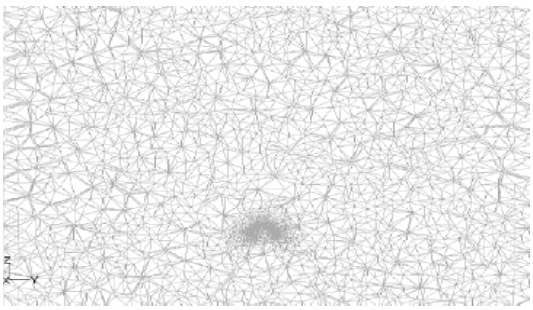

Figure 2A: FD Mesh points Figure

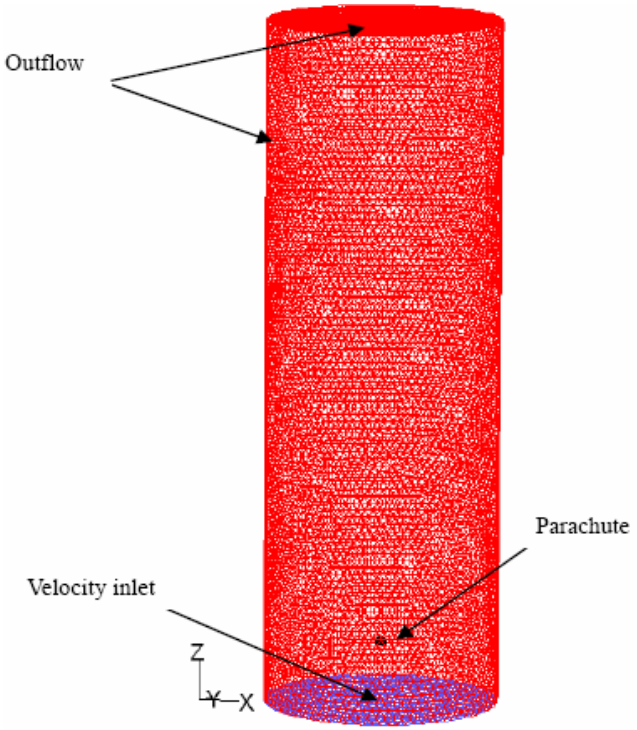

Figure 2B: Boundary conditions

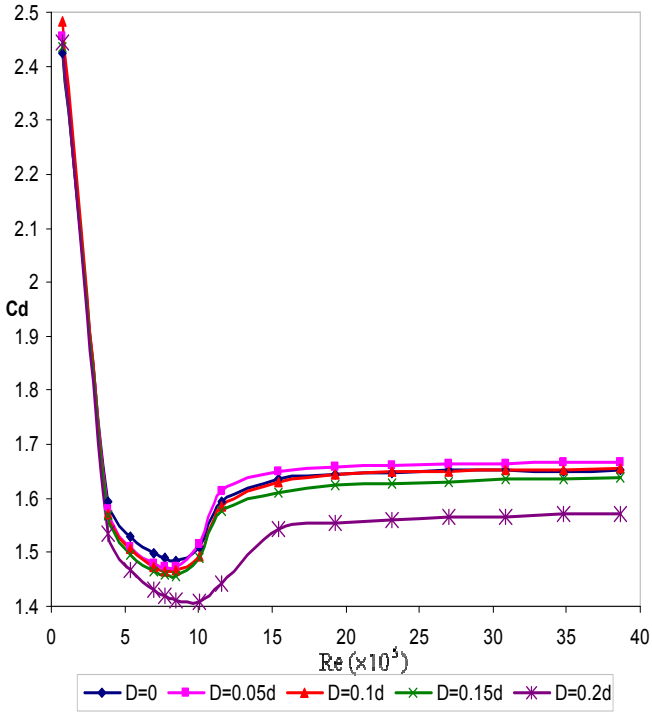

Figure 3: The drag coefficient as function of Reynolds number

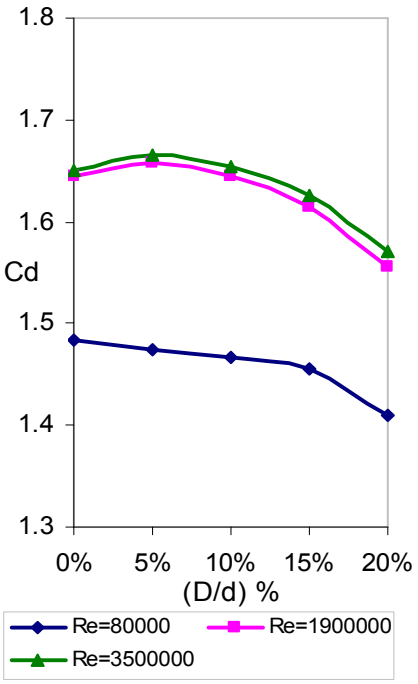

Figure 4: Drag coefficient for different vent ratios in three Reynolds number

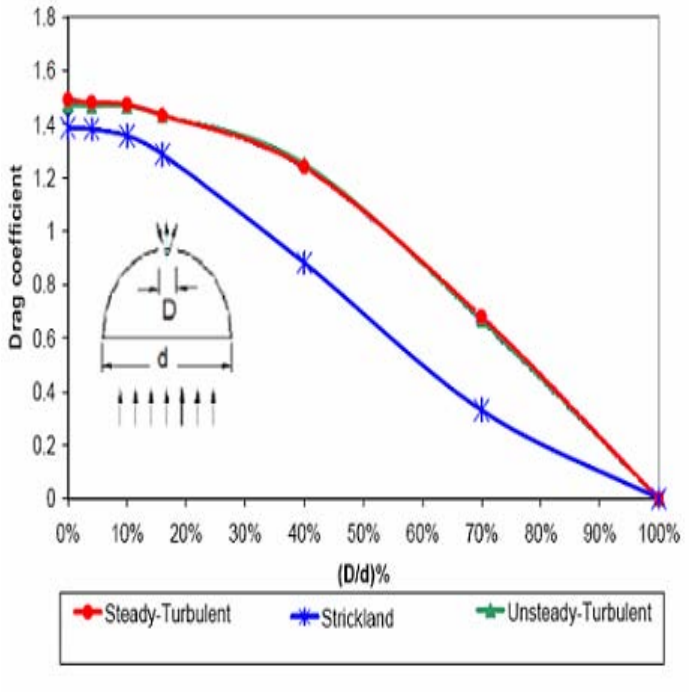

Figure 5: other software results and data gained by Strickland (Re = 788930)

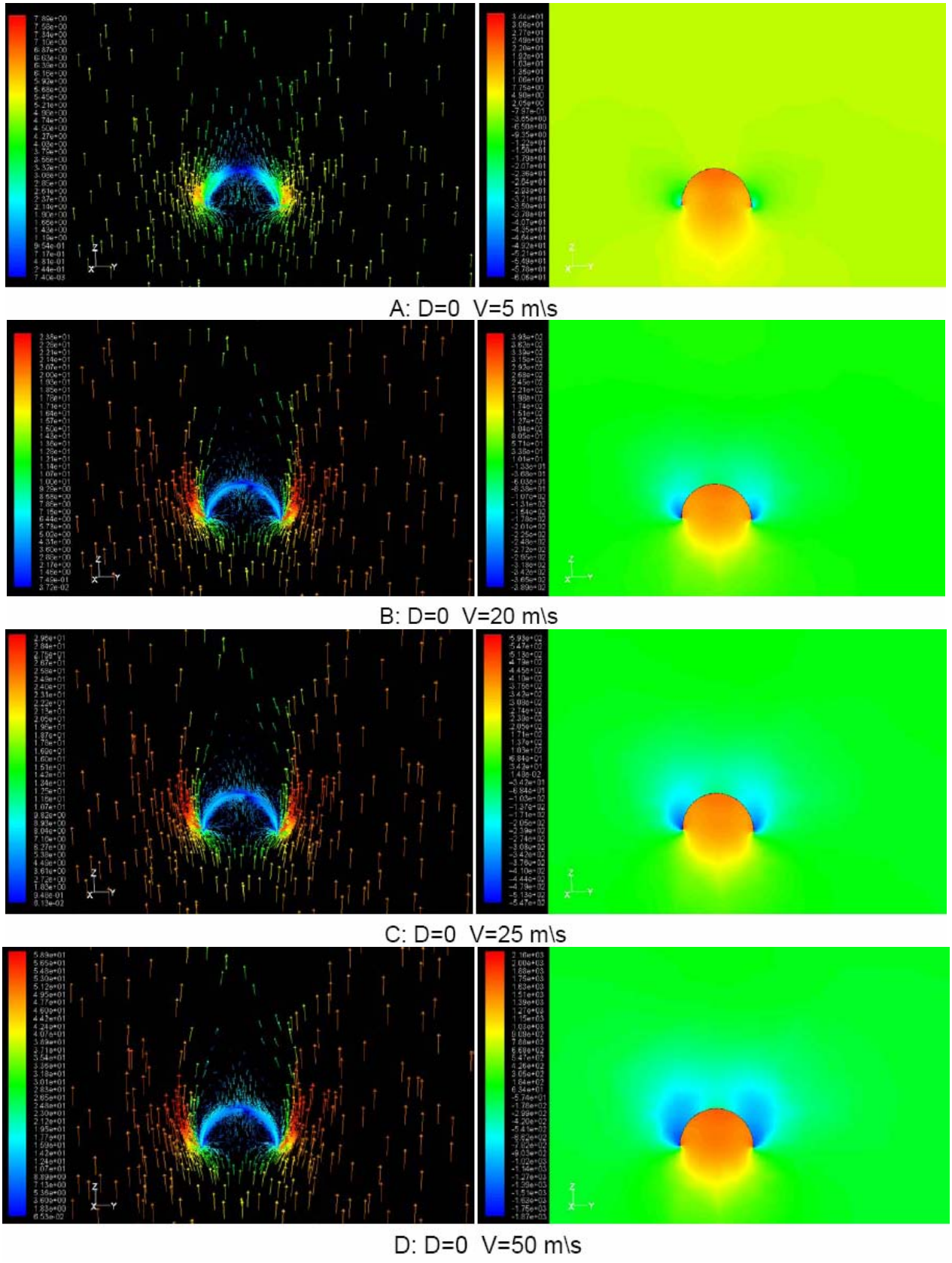

Figure 6: The velocity vectors (left) and pressure contours (right) around a hemispherical shell

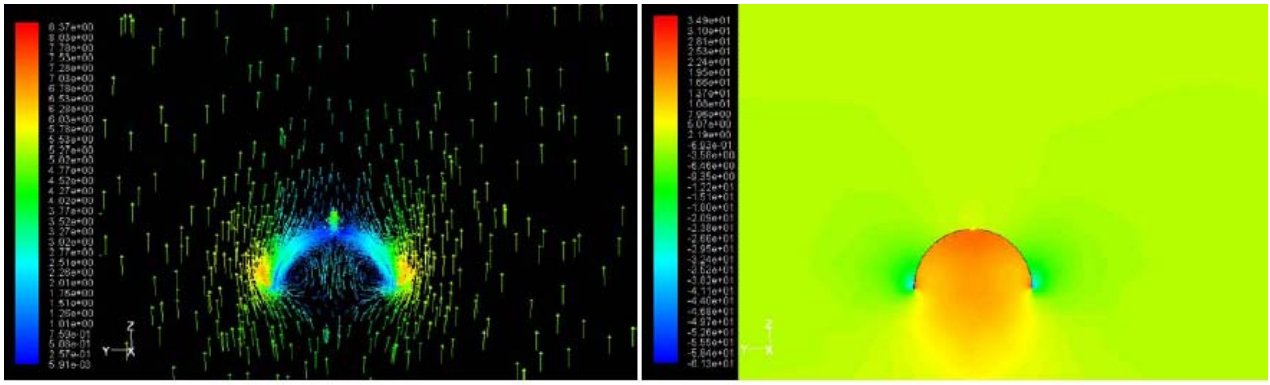

A: D=5%d V=5 m\s

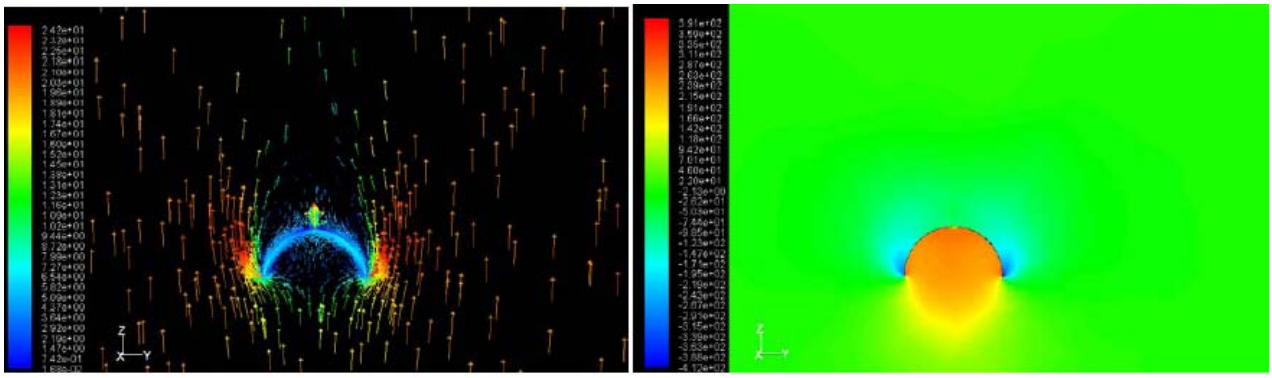

B: D=5%d V=20 m\s

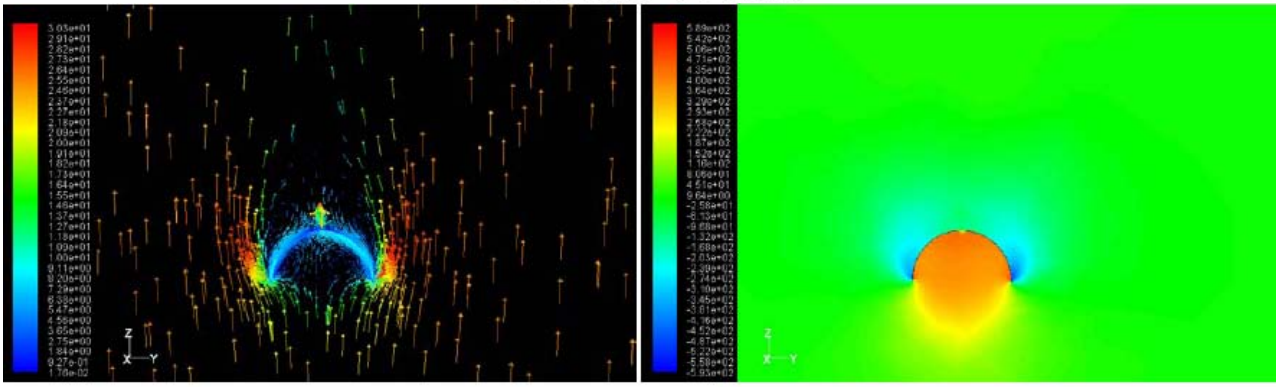

C: D=5%d V=25 m\s

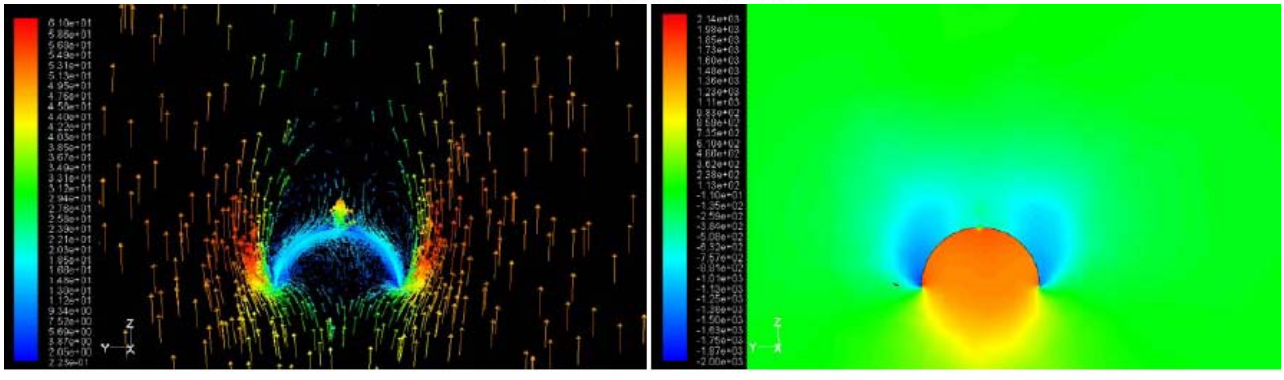

D: D=5%d V=50 m\s

Figure 7: The velocity vectors (left) and pressure contours (right) around a hemispherical shell

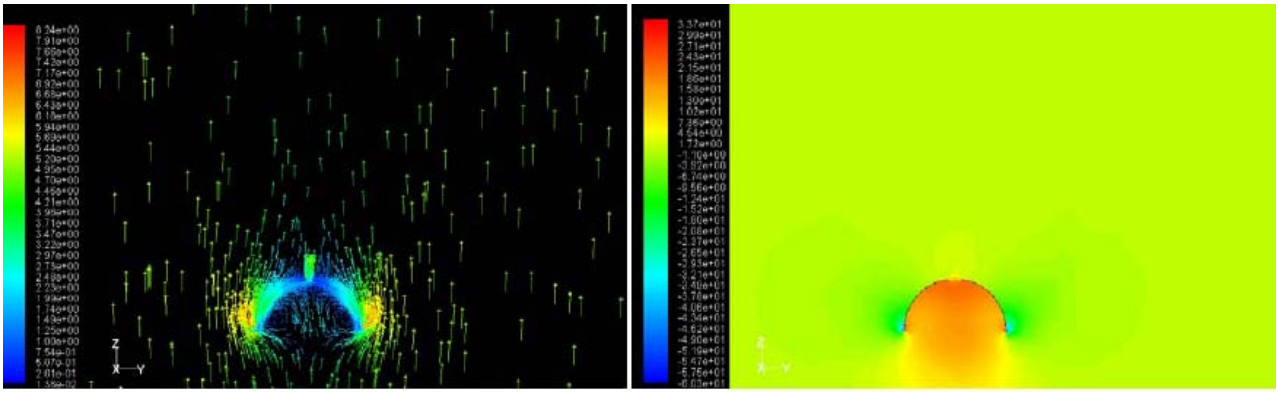

A: D=10%d V=5 m\s

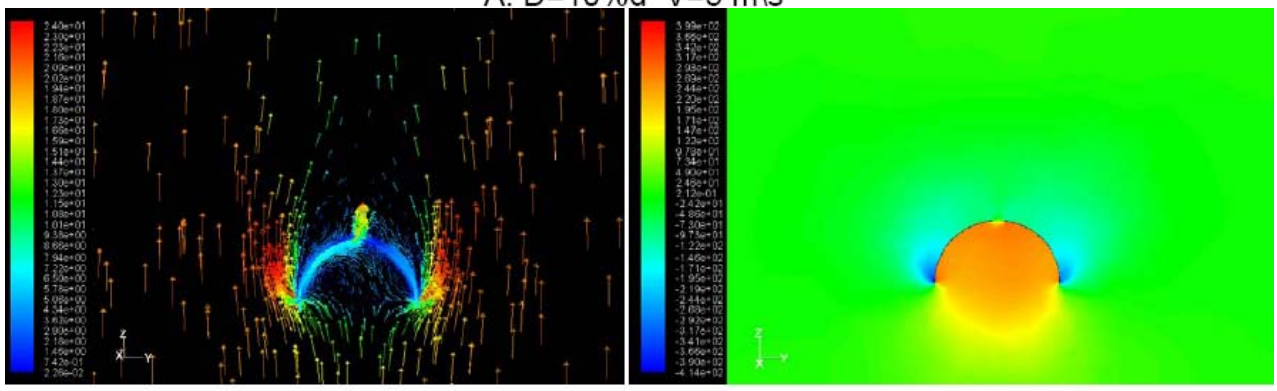

B: D=10%d V=20 m\s

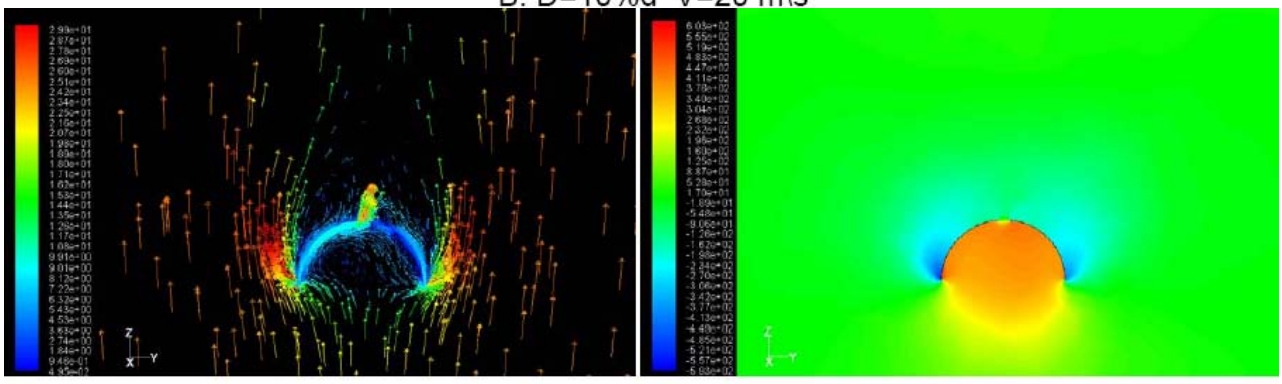

C: D=10%d V=25 m\s

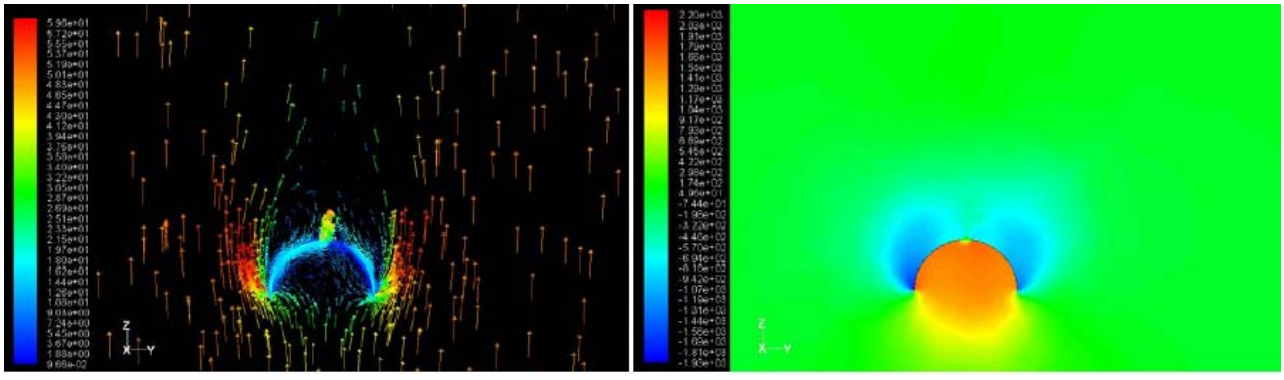

D: D=10%d V=50 m\s

Figure 8: The velocity vectors (left) and pressure contours (right) around a hemispherical shell

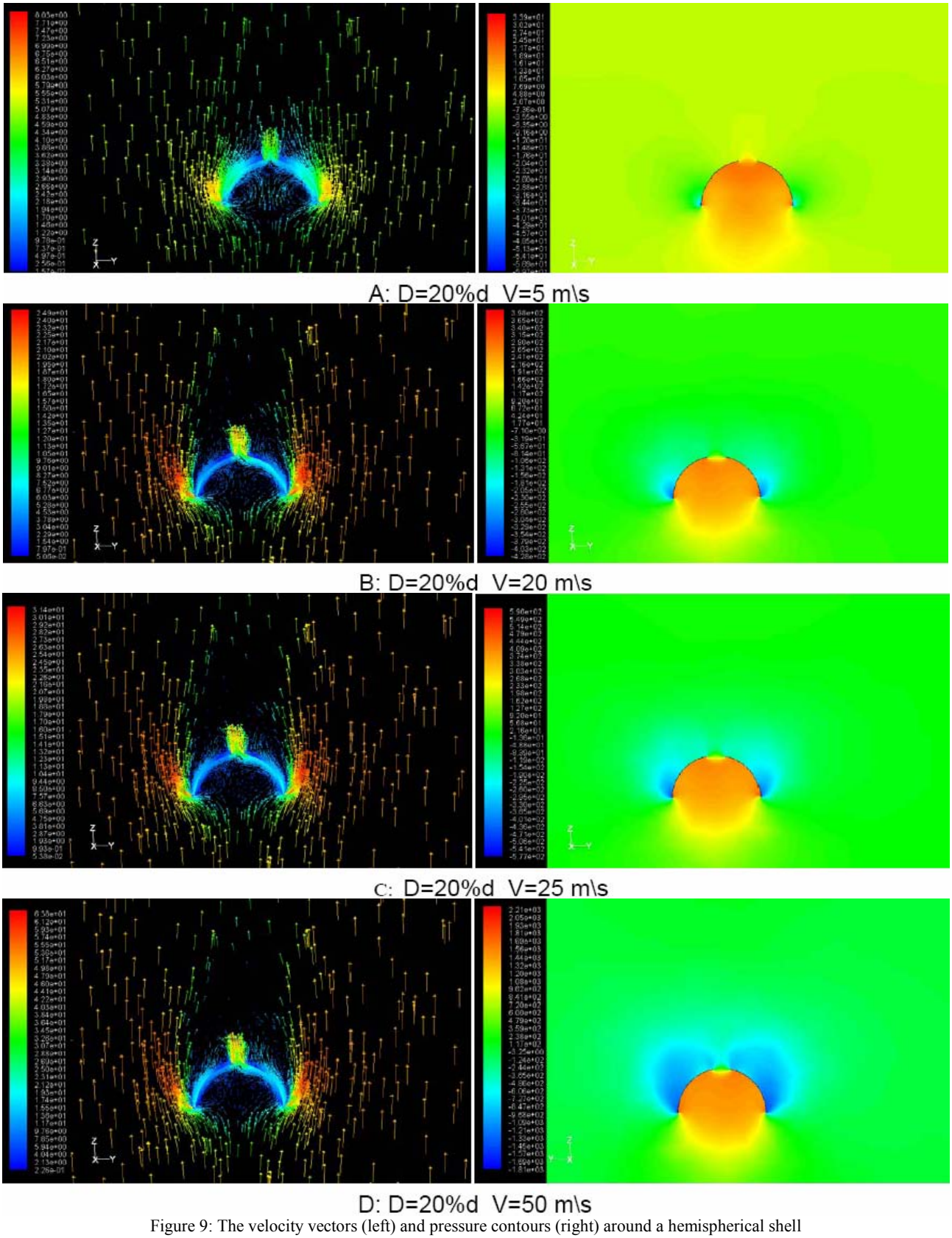

Figure 9: The velocity vectors (left) and pressure contours (right) around a hemispherical shell